

---

# Ouroboros3D: Image-to-3D Generation via 3D-aware Recursive Diffusion

---

Hao Wen<sup>1,2\*</sup> Zehuan Huang<sup>1,3\*</sup> Yaohui Wang<sup>2</sup> Xinyuan Chen<sup>2</sup> Yu Qiao<sup>2</sup> Lu Sheng<sup>1†</sup>  
<sup>1</sup>Beihang University <sup>2</sup>Shanghai AI Laboratory <sup>3</sup>VAST  
 \*Equal contribution <sup>†</sup>Corresponding author

## Abstract

Existing single image-to-3D creation methods typically involve a two-stage process, first generating multi-view images, and then using these images for 3D reconstruction. However, training these two stages separately leads to significant data bias in the inference phase, thus affecting the quality of reconstructed results. We introduce a unified 3D generation framework, named Ouroboros3D, which integrates diffusion-based multi-view image generation and 3D reconstruction into a recursive diffusion process. In our framework, these two modules are jointly trained through a self-conditioning mechanism, allowing them to adapt to each other’s characteristics for robust inference. During the multi-view denoising process, the multi-view diffusion model uses the 3D-aware maps rendered by the reconstruction module at the previous timestep as additional conditions. The recursive diffusion framework with 3D-aware feedback unites the entire process and improves geometric consistency. Experiments show that our framework outperforms separation of these two stages and existing methods that combine them at the inference phase. Project page: <https://costwen.github.io/Ouroboros3D/>.

## 1 Introduction

3D content creation from a single image have improved rapidly in recent years with the adoption of large 3D datasets [1, 2, 3] and diffusion models [4, 5, 6]. A body of research [7, 8, 9, 10, 11, 12, 13, 14] has focused on multi-view diffusion models, fine-tuning pretrained image or video diffusion models on 3D datasets to enable consistent multi-view synthesis. These methods demonstrate generalizability and produce promising results. Another group of works [15, 16, 17, 18, 19] propose generalizable reconstruction models, generating 3D representation from one or few views in a feed-forward process, which has led to efficient image-to-3D creation.

Since single-view reconstruction models [15] trained on 3D datasets [1, 20] lack generalizability and often produce blurring at unseen viewpoints, several works [21, 16, 18, 19] combine multi-view diffusion models and feed-forward reconstruction models, so as to extend the reconstruction stage to sparse-view input, boosting the reconstruction quality. As shown in Fig. 1, these methods split 3D generation into two stages: multi-view synthesis and 3D reconstruction. By combining generalizable multi-view diffusion models and robust sparse-view reconstruction models, such pipelines achieve high-quality image to 3D generation. However, combining the two independently designed models introduces a significant “data bias” to the reconstruction model. The data bias is mainly reflected in two aspects: **(1) Multi-view bias.** Multi-view diffusion models learn consistency at the image level, which makes it difficult to ensure geometric consistency. When it comes to reconstruction, multi-view images that lack geometric consistency affect the subsequent stage. **(2) Limited data for reconstruction model.** Unlike multi-view diffusion models, reconstruction models which are trained from scratch on limited 3D dataset, lacks the generalization ability.

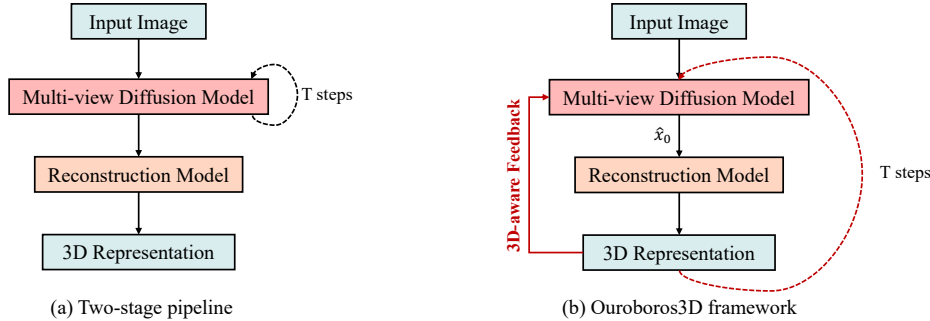


Figure 1: **Concept comparison** between Ouroboros3D and previous two-stage methods. Instead of separating multi-view diffusion model and reconstruction model, our framework involves joint training and inference of these two models, which are established into a recursive diffusion process.

Recent works like IM-3D [22] and VideoMV [23] have attempted to aggregate the rendered views of the reconstructed 3D model into multi-view synthesis by adopting re-sampling strategy in the denoising loop, thus improving the consistency of the generated multi-view images. These methods integrate the aforementioned two stages at the inference phase. But the models at both stages still lack joint training, which prevents the reconstruction model from enhancing its robustness to the generated multi-view images. Moreover, these test-time aggregating methods cannot directly utilize geometric information such as depth maps, normal maps, or coordinates maps [24] that can also be obtained from the reconstructed 3D. Notably, these explicit 3D aware maps can better guide the multi-view generation.

In this paper, we propose a unified image-to-3D creation framework, Ouroboros3D, which integrates multi-view generation and 3D reconstruction into a recursive diffusion process (shown in Fig. 2). Our framework jointly trains the multi-view diffusion model and the reconstruction model through a self-conditioning mechanism, allowing them to adapt to each other’s characteristics for robust inference. During multi-view denoising, the multi-view diffusion model uses the 3D-aware maps rendered by the reconstruction module at the previous timestep as additional conditions. By leveraging color maps and spatial canonical coordinates maps from the reconstructed 3D representation, our multi-view diffusion model generates images that better conform to the actual 3D structure. This recursive diffusion framework enhances generating complex scenes by uniting the 3D generation process with 3D-aware feedback. In our experiments, we use the video diffusion model [25] as the multi-view generator and the Large Multi-View Gaussian Model (LGM) [16] as the reconstruction module. Tests on the GSO dataset [26] show that our framework outperforms separation of these stages and existing methods [23] that combine the stages at the inference phase.

Our key contributions are as follows:

- We introduce a image-to-3D creation framework Ouroboros3D, which integrates multi-view generation and 3D reconstruction into a recursive diffusion process.
- Ouroboros3D employs a self-conditioning mechanism with 3D-aware feedback, using rendered maps to guide the multi-view generation, ensuring better geometric consistency and robustness.
- Experiments show that our framework significantly reduces data bias, and outperforms separation of the two stages and existing methods [23] that combine the stages at the inference stage.

## 2 Related Work

**Image/Video Diffusion for Multi-view Generation** Diffusion models [27, 28, 29, 30, 31, 32, 33, 25, 34, 35] have demonstrated their powerful generative capabilities in image and video generation fields. Current research [7, 8, 9, 10, 11, 12, 13, 14, 36] fine-tunes pretrained image/video diffusion models on 3D datasets like Objaverse [1] and MVImageNet [20]. Zero123 [7] introduces relative view condition to image diffusion models, enabling novel view synthesis from a single image and preserving generalizability. Based on it, methods like SyncDreamer [9], ConsistNet [37] and EpiDiff [11] design attention modules to generate consistent multi-view images. These methods fine-

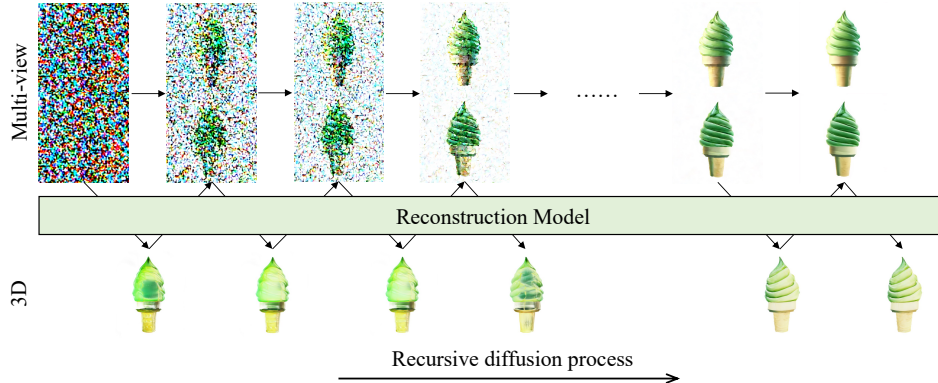


Figure 2: **Overview of 3D-aware recursive diffusion.** During multi-view denoising, the diffusion model uses 3D-aware maps rendered by the reconstruction module at the previous step as conditions.

tuned from image diffusion models produce generally promising results. By considering multi-view images as consecutive frames of a video (e.g., orbiting camera views), it naturally leads to the idea of applying video generation models to 3D generation [13]. However, since the diffusion model is not explicitly modeled in 3D space, the generated multi-view images often struggle to achieve consistent and robust details.

**Image to 3D Reconstruction** Recently, the task of reconstructing 3D objects has evolved from traditional multi-view reconstruction methods [38, 39, 40, 41] to feed-forward reconstruction models [15, 42, 43, 16, 17, 18, 19]. Utilizing one or few shot as input, these highly generalizable reconstruction models synthesize 3D representation, enabling the rapid generation of 3D objects. LRM [15] proposes a transformer-based model to effectively map image tokens to 3D triplanes. Instant3D [21] further extends LRM to sparse-view input, significantly boosting the reconstruction quality. LGM [16] and GRM [17] replace the triplane representation with 3D Gaussians [41] to enjoy its superior rendering efficiency. CRM [18] and InstantMesh [19] optimize on the mesh representation for high-quality geometry and texture modeling. These reconstruction models built upon convolutional network architecture or transformer backbone, have led to efficient image-to-3D creation.

**Pipelines of 3D Generation** Early works propose to distill knowledge of image prior to create 3D models via Score Distillation Sampling (SDS) [44, 45, 46], limited by the low speed of per-scene optimization. Several works [9, 11, 14, 22] fine-tune image diffusion models to generate multi-view images, which are then utilized for 3D shape and appearance recovery with traditional reconstruction methods [47, 41]. More recently, several works [21, 16, 18, 19, 23] involve both multi-view diffusion models and feed-forward reconstruction models in the generation process. Such pipelines attempt to combine the processes into a cohesive two-stage approach, thus achieving highly generalizable and high-quality single-image to 3D generation. However, due to the lack of explicit 3D modeling, the results generated by the multi-view diffusion model cannot guarantee strong consistency, which will lead to data deviation for the reconstructed model between the testing phase and the training phase. Compared to them, we propose a unified pipeline, integrating the two stages through a self-conditioning mechanism at the training stage, with 3D aware feedback for high consistency.

### 3 Method

Given a single image, Ouroboros3D aims to generate multiview-consistent images with a reconstructed 3D Gaussian model. To reduce the data bias and improve robustness of the generation, our framework integrates multi-view synthesis and 3D reconstruction in a recursive diffusion process. As illustrated in Fig. 3, the proposed framework involves a video diffusion model (SVD [25]) as multi-view generator (refer to Section 3.1) and a feed-forward reconstruction model to recover a 3D Gaussian Splatting (refer to Section 3.2). Moreover, we introduce a self-conditioning mechanism, feeding the 3D-aware information obtained from the reconstruction module back to the multi-view

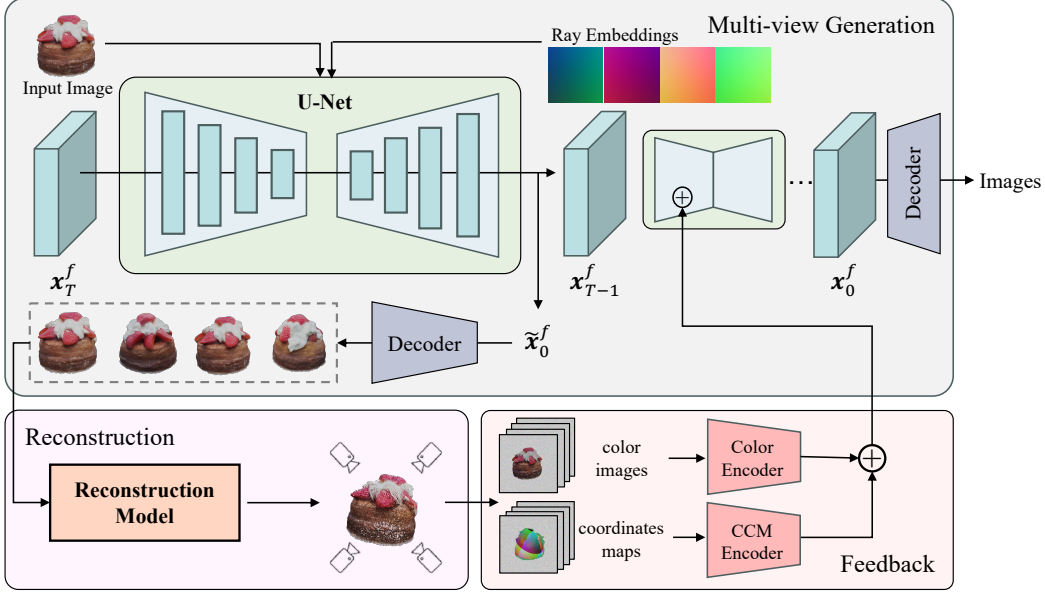


Figure 3: **Overview of Ouroboros3D.** We adopt a video diffusion model as the multi-view generator by incorporating the input image and relative camera poses. In the denoising sampling loop, we decode the predicted  $\tilde{x}_0^f$  to noise-corrupted images, which are then used to recover 3D representation by a feed-forward reconstruction model. Then the rendered color images and coordinates maps are encoded and fed into the next denoising step. At inference, the 3D-aware denoising sampling strategy iteratively refines the images by incorporating feedback from the reconstructed 3D into the denoising loop, enhancing multi-view consistency and image quality.

generation process (refer to Section 3.3). The 3D-aware recursive diffusion strategy iteratively refines the multi-view images and the 3d model, thus enhancing the final production.

### 3.1 Video Diffusion Model as Multiview Generator

Recent video diffusion models [13, 35] have demonstrated a remarkable capability to generate 3D-aware videos. We employ the well-known Stable Video Diffusion (SVD) Model as our multi-view generator, which generates videos from an image input. Further details about SVD can be found in Appendix A.1. In our framework, we set the number of the generated frames  $f$  to 8.

We enhance the video diffusion model with camera control  $c$  to generate images from different viewpoints. Traditional methods encode camera positions at the frame level, which results in all pixels within one view sharing the same positional encoding [48, 13]. Building on the innovations of previous work [11, 36], we integrate the camera condition  $c$  into the denoising network by parameterizing the rays  $\mathbf{r} = (o, o \times d)$ . Specifically, we use two-layered MLP to inject Plücker ray embeddings for each latent pixel, enabling precise positional encoding at the pixel level. This approach allows for more detailed and accurate 3D rendering, as pixel-specific embedding enhances the model’s ability to handle complex variations in depth and perspective across the video frames.

In our framework, unlike existing two-stage methods, our multi-view diffusion model does not complete all the denoising steps independently. In contrast, in the denoising sampling loop, we obtain the straightly predicted  $\tilde{x}_0^f$  at each timestep, which will be used for subsequent 3D reconstruction, and rendered maps will be used as conditions to guide the next denoising step. Therefore, at each sampling step, we do the reparameterization of the output from the denoising network  $F_\theta$  to convert it into  $\tilde{x}_0^f$ . Taking one view as an example, we use the following formula to process the denoised image  $c_{\text{in}}(\sigma)\mathbf{x}$  and the associated noise level  $c_{\text{noise}}(\sigma)$ :

$$\tilde{\mathbf{x}}_0 = c_{\text{skip}}(\sigma)\mathbf{x} + c_{\text{out}}(\sigma)F_\theta(c_{\text{in}}(\sigma)\mathbf{x}; c_{\text{noise}}(\sigma)). \quad (1)$$

where  $\sigma$  indicates the standard deviation of the noise. The above operation adjusts the output of  $F_\theta$  to  $\tilde{x}_0^f$ , which will be decoded into images and passed to the subsequent 3D reconstruction module.

### 3.2 Feed-Forward Reconstruction Model

In the Ouroboros3D framework, the feed-forward reconstruction model is designed to recover 3D models from pre-generated multi-view images, which can be images decoded from straightly predicted  $\tilde{\mathbf{x}}_0^f$ , or completely denoised images. We utilize Large Multi-View Gaussian Model (LGM) [16]  $\mathcal{G}$  as our reconstruction module due to its real-time rendering capabilities that benefit from 3D representation of Gaussian Splatting. This method integrates seamlessly with our jointly training framework, allowing for quick adaptation and efficient processing.

We pass four specific views from the reparameterized output  $\tilde{\mathbf{x}}_0^f$  to the Large Gaussian Model (LGM) for 3D Gaussian Splatting reconstruction. To enhance the performance of LGM, particularly its sensitivity to different noise levels  $c_{\text{noise}}(\sigma)$  and image details, we introduce a zero-initialized time embedding layer within the original U-Net structure of the LGM. This innovative modification enables the LGM to dynamically adapt to the diverse outputs that arise at different stages of the denoising process, thereby substantially improving its capacity to accurately reconstruct 3D content from images that have undergone partial denoising.

The loss function employed for the fine-tuning of the LGM is articulated as follows:

$$\mathcal{L}_G = \mathcal{L}_{\text{rgb}}(\mathbf{x}_0, \mathcal{G}(\tilde{\mathbf{x}}_0, c_{\text{noise}}(\sigma))) + \lambda \mathcal{L}_{\text{LPIPS}}(\mathbf{x}_0, \mathcal{G}(\tilde{\mathbf{x}}_0, c_{\text{noise}}(\sigma))). \quad (2)$$

where we have utilized the mean square error loss  $\mathcal{L}_{\text{rgb}}$  for the color channel and a VGG-based perceptual loss  $\mathcal{L}_{\text{LPIPS}}$  for the LPIPS term. In practical applications, the weighting factor  $\lambda$  is conventionally set to 1.

Additionally, to maintain the model’s reconstruction capability for normal images, we also input the model without adding noise and calculate the corresponding loss. In this case, we set  $c_{\text{noise}}(\sigma)$  to 0.

### 3.3 3D-Aware Feedback Mechanism

As shown in Fig. 3, we adopt a 3D-aware feedback mechanism that involves the rendered color images and geometric maps produced by our reconstruction module in a denoising loop to further improve the multi-view consistency of the resulting images and facilitate cyclic adaptation of the two stages. Instead of integrating multi-view generation and 3D reconstruction at the inference stage using re-sampling strategy [22, 23], we propose to train these two modules jointly to support more informative feedback. Specifically, in addition to the rendered color images, our flexible framework is able to derive additional geometric features to guide the generation process, which brings guidance of more explicit 3D information to multi-view generation.

In practice, we obtain color images and canonical coordinates maps (CCM) [24] from the reconstructed 3D model, and utilize them as condition to guide the next denoising step of multi-view generation. We use position maps instead of depth maps or normal maps as the representative of geometric maps because canonical coordinate maps record the global vertex coordinate values after normalization of the overall 3D model, rather than the normalization of the relative self-view (such as depth maps). This operation enables the rendered maps to be characterized as cross-view alignment, providing the strong guidance of more explicit cross-view geometry relationship. The details of canonical coordinates maps can be found in Appendix A.2.

To encode color images and coordinates maps into the denoising network of multi-view generation module, we design two simple and lightweight encoders for color images and coordinates maps using a series of convolutional neural networks, like T2I-Adapter [49]. The encoders are composed of four feature extraction blocks and three downsample blocks to change the feature resolution, so that the dimension of the encoded features is the same as the intermediate feature in the encoder of U-Net denoiser. The extracted features from the two conditional modalities are then added to the U-Net encoder at each scale.

We propose a 3D-aware self-conditioning [50] training and inference strategy. The original multi-view denoising network  $F_\theta(\mathbf{x}; \sigma)$  is augmented with 3D-aware feedback, formulated as  $F_\theta(\mathbf{x}; \sigma, \mathcal{G}(\tilde{\mathbf{x}}_0))$ , where  $\mathcal{G}(\tilde{\mathbf{x}}_0)$  is the rendered maps of the reconstruction module.

**Training Strategy** As illustrated in Algorithm 1, to train a 3D-aware multi-view generation network, we use the rendered results from feed-forward model as the self-conditioning input. In practice, we

randomly apply this mechanism with a probability of 0.5. When not using the 3D reconstruction result, we set  $\mathcal{G}(\tilde{x}_0) = 0$  as the input. This probabilistic approach ensures balanced learning, allowing the model to effectively incorporate 3D information without over-reliance on it.

---

**Algorithm 1** Training Ouroboros3D with the self-conditioned strategy.

---

```
def train_loss(x, cond_image):
    """Returns the loss on a training example x."""
    # Sample sigma from a log-normal distribution and init the self_cond
    sigma, self_cond = log_normal(P_mean, P_std), None

    # Reparameterize sigma to obtain conditioning parameters
    c_in, c_out, c_skip, c_noise, lambda_param = reparameterizing(sigma)

    # Add noise to input data
    noise_x = x + sigma * normal(mean=0, std=1)
    input_x = c_in * noise_x

    pred_x = c_out * net(input_x, c_noise, cond_image, self_cond) + c_skip * noise_x

    # Update self_cond using the reconstruction model
    self_cond = recon_model(pred_x, c_noise)

    # Use rendered maps as condition and denoise
    if self_cond and random_uniform(0, 1) > 0.5:
        pred_x = c_out * net(input_x, t, cond_image, self_cond.detach()) + c_skip *
        ↪ noise_x

    # Compute loss
    loss = lambda_param * (pred_x - target) ** 2
    recon_loss = recon_loss_fn(self_cond, x)

    return loss.mean() + recon_loss
```

---

**Inference/Sampling Strategy** At the inference stage, as shown in Algorithm 2, the 3D feedback  $\mathcal{G}(\tilde{x}_0)$  is initially set to 0. At subsequent timesteps, this condition is updated with the previous reconstruction result  $\mathcal{G}(\tilde{x}_0)$ . This iterative process refines the 3D representation, ensuring each frame benefits from prior reconstructions, leading to more consistent multi-view images and higher quality reconstructed 3D models.

---

**Algorithm 2** Sampling algorithm of Ouroboros3D.

---

```
def generate(sigmas, cond_image):
    self_cond = None
    x_T = normal(mean=0, std=1) # Initialize latent variable with Gaussian noise
    for sigma in sigmas:
        # Reparameterize sigma to obtain conditioning parameters
        c_in, c_out, c_skip, c_noise, lambda_param = reparameterizing(sigma)

        # Add noise to the latent variable
        noise_x = x_T + sigma * normal(mean=0, std=1)
        input_x = c_in * noise_x

        # Generate prediction
        F_pred = net(input_x, t, cond_image, self_cond)
        pred_x = c_out * F_pred + c_skip * noise_x

        # Update self_cond using the reconstruction model
        self_cond = recon_model(pred_x, c_noise)

    return pred_x, self_cond
```

---

|                    | Method                  | Resolution       | PSNR $\uparrow$ | SSIM $\uparrow$ | LPIPS $\downarrow$ |
|--------------------|-------------------------|------------------|-----------------|-----------------|--------------------|
| Image-to-Multiview | SyncDreamer [9]         | 256 $\times$ 256 | 20.056          | 0.8163          | 0.1596             |
|                    | SV3D [13]               | 576 $\times$ 576 | 21.042          | 0.8497          | 0.1296             |
|                    | VideoMV [23]            | 256 $\times$ 256 | 18.605          | 0.8410          | 0.1548             |
|                    | Ouroboros3D (SVD)       | 512 $\times$ 512 | <b>21.770</b>   | <b>0.8866</b>   | <b>0.1093</b>      |
| Image-to-3D        | TripoSR [53]            | 256 $\times$ 256 | 18.481          | 0.8506          | 0.1357             |
|                    | LGM [16]                | 512 $\times$ 512 | 17.716          | 0.8319          | 0.1894             |
|                    | VideoMV(GS) [23]        | 256 $\times$ 256 | 18.764          | 0.8449          | 0.1569             |
|                    | InstantMesh (NeRF) [19] | 512 $\times$ 512 | 19.948          | 0.8727          | 0.1205             |
|                    | Ouroboros3D (LGM)       | 512 $\times$ 512 | <b>21.761</b>   | <b>0.8894</b>   | <b>0.1091</b>      |

Table 1: Quantitative comparison on the quality of generated multi-view images and 3D representation for image-to-multiview and image-to-3D tasks.

## 4 Experiments

### 4.1 Implementation Details

**Datasets** We use a filtered subset of the Objaverse [1] dataset to train our model, following LGM [16] to remove bad models with bad captions or missing texture. It leads to a final set of around 80K 3D objects. We render 2 16-frame RGBA orbits at 512  $\times$  512. For each orbit, the cameras are positioned at a randomly sampled elevation between [-5, 30] degrees. During training, we subsample any 8-frame orbit by picking any frame in one orbit as the first frame (the conditioning image), and then choose every 2nd frame after that.

We evaluate the synthesized multi-view images and reconstructed 3D Gaussian Splatting (3DGS) on the unseen GSO [26] dataset. We filter 100 objects to reduce redundancy and maintain diversity. For each object, we render ground truth orbit videos and pick the first frame as the conditioning image.

**Experimental Settings** Our Ouroboros3D is trained for 30,000 iterations using 8 A100 GPUs with a total batch size of 32. We clip the gradient with a maximum norm of 1.0. We use the AdamW optimizer with a learning rate of  $1 \times 10^{-5}$  and employ FP16 mixed precision with DeepSeed[51] with Zero-2 for efficient training. At the inference stage, we set the number of sampling steps as 25, which takes about 20 seconds to generate a 3d model.

**Metrics** We compare generated multi-view images and rendered views from reconstructed 3DGS with the ground truth frames, in terms of Learned Perceptual Similarity (LPIPS [52]), Peak Signal-to-Noise Ratio (PSNR), and Structural SIMilarity (SSIM).

**Baselines** In terms of multi-view generation, we compare Ouroboros3D with SyncDreamer [9], SV3D [13], VideoMV [23]. For image-to-3D creation, we adopt feed-forward reconstruction models or pipelines as baseline methods, including TripoSR [53], LGM [16] and InstantMesh [19]. Notably, LGM and InstantMesh adopt two-stage methods to achieve image-to-3D creation, which generate multi-view images and then utilize large reconstruction models to obtain 3D objects.

### 4.2 Comparison with Existing Alternatives

**Image-to-Multiview** We first compare against recent image-to-multiview generation methods [9, 13, 23]. The quantitative results are shown in Table 1, and the qualitative results are shown in Fig. 4. The multi-view images produced by ours have better quality and consistency than those which train the multi-view generator independently or leverage reconstruction models to improve consistency at inference.

**Image-to-3D** We then compare with recent methods [53, 16, 23, 19] on image-to-3D tasks that are capable of generating 3D Gaussians or other 3D representation like triplane NeRF. Fig. 5 shows images rendered from the generated 3D for comparison. We also present the quantitative results in Table 1. We observe that our unified framework generates more realistic and high-quality 3D objects than existing methods which separate the two stages of multi-view generation and 3D reconstruction, or unites them at the inference stage. More results are shown in Fig. 8.

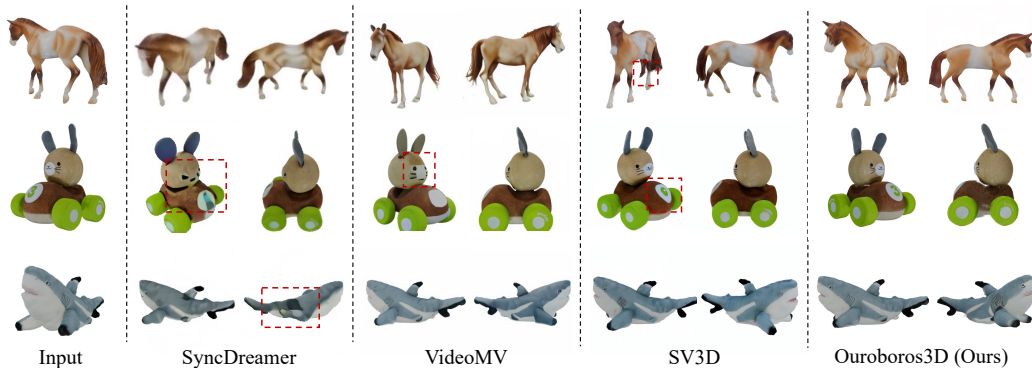


Figure 4: Qualitative comparisons of generated multi-view images. Our method achieves better consistency and quality.

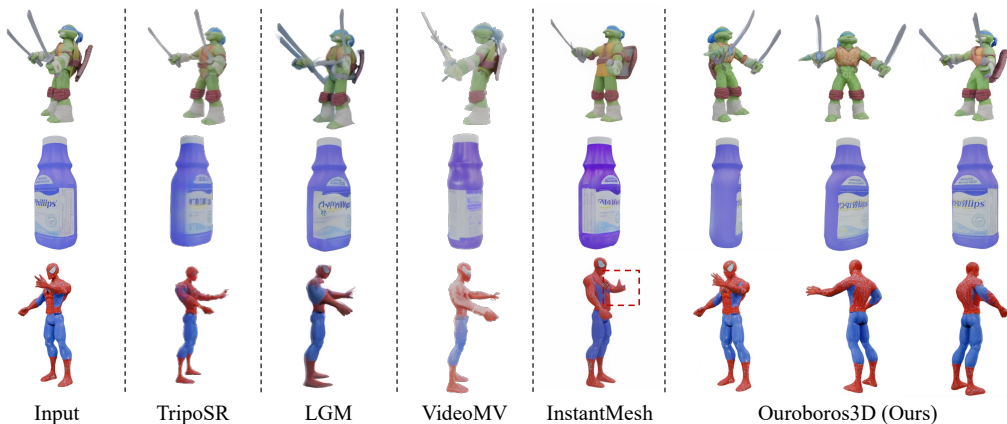


Figure 5: Qualitative comparisons for image-to-3D.

**Generalizability** Our method is applicable to image inputs outside the distribution and can produce high-quality objects with the consistent 3D structure, as results are shown in Fig. 6 and Fig. 8.

### 4.3 Ablation Study

To assess the effectiveness of our 3D-aware feedback mechanism, we conducted ablation experiments on the generated 3DGS for different configurations (Fig. 7 and Table 2). We start with a “base framework” that does not jointly trains the multi-view generation module and the reconstruction module, or use feedback mechanism. We then incrementally add components of our proposed approach. The full model (the last setting) means that we use both geometry and appearance information as conditions to guide the multi-view generation. Table 2 reports the ablation results, which demonstrate significant improvements by enhancing both geometric consistency and texture details. We also report the absolute distances of performance metrics between the generated multiviews and 3DGS.

| Jointly Training | Feedbacks | PSNR $\uparrow$ | SSIM $\uparrow$ | LPIPS $\downarrow$ | $\Delta$ PSNR $\downarrow$ | $\Delta$ SSIM $\downarrow$ | $\Delta$ LPIPS $\downarrow$ |
|------------------|-----------|-----------------|-----------------|--------------------|----------------------------|----------------------------|-----------------------------|
| $\times$         | $\times$  | 20.012          | 0.8465          | 0.1287             | 1.067                      | 0.0125                     | 0.0189                      |
| $\checkmark$     | $\times$  | 20.549          | 0.8651          | 0.1221             | 0.511                      | 0.0094                     | 0.0070                      |
| $\checkmark$     | CCM       | 21.325          | 0.8738          | 0.1192             | 0.304                      | 0.0036                     | 0.0018                      |
| $\checkmark$     | CCM + RGB | <b>21.761</b>   | <b>0.8894</b>   | <b>0.1091</b>      | <b>0.009</b>               | <b>0.0028</b>              | <b>0.0002</b>               |

Table 2: Ablation study of different feedback mechanisms. Results show that our 3D-aware feedback mechanism lead to superior generalization performance.



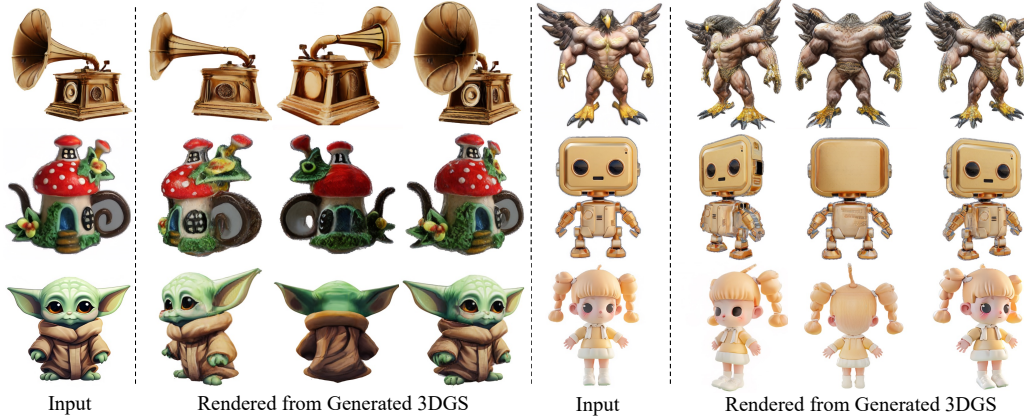


Figure 6: Generalizability of our 3D generation. We can generate high-quality 3D models given image inputs outside the distribution.

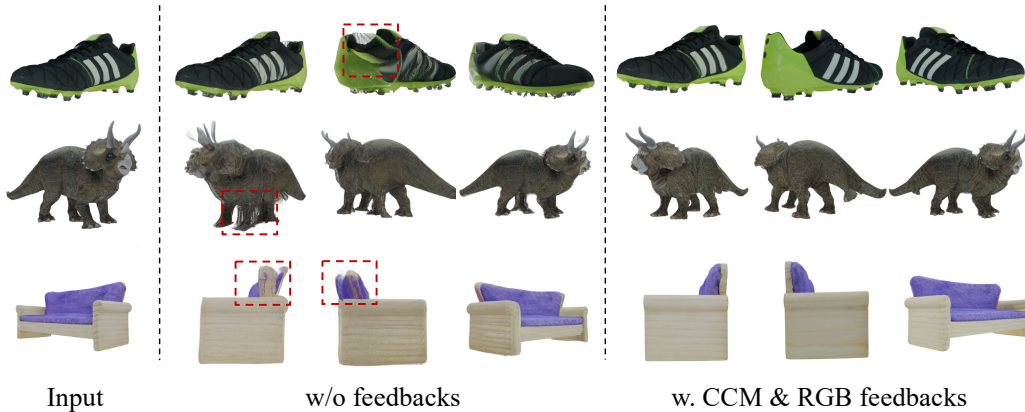


Figure 7: Qualitative comparison with no-feedback and 3d-aware feedback.

It can be observed that our framework reduces the performance difference between the generated multi-view images and 3D representation, and improves the combined performance.

#### 4.4 Limitations and Future Works

Our model currently utilize 3D Gaussian splating as the generated 3D representation, which is not as widely used in the gaming field as meshes. Replacing the reconstruction module with CRM [18] or InstantMesh [19] can enable our framework to generate meshes from a single image. In addition, experiments on 3D scene dataset will also be an extension of our framework.

## 5 Conclusion

In this paper, we introduce Ouroboros3D, a unified framework for single image-to-3D creation that integrates multi-view image generation and 3D reconstruction in a recursive diffusion process. We In our framework, these two modules are jointly trained through a self-conditioning mechanism, which allows them to adapt to the inherent characteristic of each stage, leading to more robust generation. By establishing a recursive relationship between these two stages through a self-conditioning mechanism, our approach effectively mitigates the data bias encountered in existing two-stage methods. Experiments demonstrate that Ouroboros3D not only generates consistent and high-quality multi-view images, but also produces 3D objects with superior geometric consistency and details.



Figure 8: More visualization results of our image-to-3D creation.

## References

- [1] Matt Deitke, Dustin Schwenk, Jordi Salvador, Luca Weihs, Oscar Michel, Eli VanderBilt, Ludwig Schmidt, Kiana Ehsani, Aniruddha Kembhavi, and Ali Farhadi. Objaverse: A universe of annotated 3d objects. In *Proceedings of the IEEE/CVF Conference on Computer Vision and Pattern Recognition*, pages 13142–13153, 2023.
- [2] Matt Deitke, Ruoshi Liu, Matthew Wallingford, Huong Ngo, Oscar Michel, Aditya Kusupati, Alan Fan, Christian Laforte, Vikram Voleti, Samir Yitzhak Gadre, et al. Objaverse-xl: A universe of 10m+ 3d objects. *Advances in Neural Information Processing Systems*, 36, 2024.
- [3] Tong Wu, Jiarui Zhang, Xiao Fu, Yuxin Wang, Jiawei Ren, Liang Pan, Wayne Wu, Lei Yang, Jiaqi Wang, Chen Qian, et al. Omniobject3d: Large-vocabulary 3d object dataset for realistic perception, reconstruction and generation. In *Proceedings of the IEEE/CVF Conference on Computer Vision and Pattern Recognition*, pages 803–814, 2023.
- [4] Jascha Sohl-Dickstein, Eric Weiss, Niru Maheswaranathan, and Surya Ganguli. Deep unsupervised learning using nonequilibrium thermodynamics. In Francis Bach and David Blei, editors, *Proceedings of the 32nd International Conference on Machine Learning*, volume 37 of *Proceedings of Machine Learning Research*, pages 2256–2265, Lille, France, 07–09 Jul 2015. PMLR.
- [5] Jonathan Ho, Ajay Jain, and Pieter Abbeel. Denoising diffusion probabilistic models. *Advances in neural information processing systems*, 33:6840–6851, 2020.
- [6] Yang Song, Jascha Sohl-Dickstein, Diederik P Kingma, Abhishek Kumar, Stefano Ermon, and Ben Poole. Score-based generative modeling through stochastic differential equations. *arXiv preprint arXiv:2011.13456*, 2020.
- [7] Ruoshi Liu, Rundi Wu, Basile Van Hoorick, Pavel Tokmakov, Sergey Zakharov, and Carl Vondrick. Zero-1-to-3: Zero-shot one image to 3d object. In *Proceedings of the IEEE/CVF International Conference on Computer Vision*, pages 9298–9309, 2023.

- [8] Yichun Shi, Peng Wang, Jianglong Ye, Mai Long, Kejie Li, and Xiao Yang. Mvdream: Multi-view diffusion for 3d generation. *arXiv preprint arXiv:2308.16512*, 2023.
- [9] Yuan Liu, Cheng Lin, Zijiao Zeng, Xiaoxiao Long, Lingjie Liu, Taku Komura, and Wenping Wang. Syncdreamer: Generating multiview-consistent images from a single-view image. *arXiv preprint arXiv:2309.03453*, 2023.
- [10] Jeong-gi Kwak, Erqun Dong, Yuhe Jin, Hanseok Ko, Shweta Mahajan, and Kwang Moo Yi. Vivid-1-to-3: Novel view synthesis with video diffusion models. *arXiv preprint arXiv:2312.01305*, 2023.
- [11] Zehuan Huang, Hao Wen, Junting Dong, Yaohui Wang, Yangguang Li, Xinyuan Chen, Yan-Pei Cao, Ding Liang, Yu Qiao, Bo Dai, et al. Epidiff: Enhancing multi-view synthesis via localized epipolar-constrained diffusion. *arXiv preprint arXiv:2312.06725*, 2023.
- [12] Shitao Tang, Jiacheng Chen, Dilin Wang, Chengzhou Tang, Fuyang Zhang, Yuchen Fan, Vikas Chandra, Yasutaka Furukawa, and Rakesh Ranjan. Mvdifffusion++: A dense high-resolution multi-view diffusion model for single or sparse-view 3d object reconstruction. *arXiv preprint arXiv:2402.12712*, 2024.
- [13] Vikram Voleti, Chun-Han Yao, Mark Boss, Adam Letts, David Pankratz, Dmitry Tochilkin, Christian Laforte, Robin Rombach, and Varun Jampani. Sv3d: Novel multi-view synthesis and 3d generation from a single image using latent video diffusion, 2024.
- [14] Xiaoxiao Long, Yuan-Chen Guo, Cheng Lin, Yuan Liu, Zhiyang Dou, Lingjie Liu, Yuexin Ma, Song-Hai Zhang, Marc Habermann, Christian Theobalt, et al. Wonder3d: Single image to 3d using cross-domain diffusion. *arXiv preprint arXiv:2310.15008*, 2023.
- [15] Yicong Hong, Kai Zhang, Jiuxiang Gu, Sai Bi, Yang Zhou, Difan Liu, Feng Liu, Kalyan Sunkavalli, Trung Bui, and Hao Tan. Lrm: Large reconstruction model for single image to 3d. *arXiv preprint arXiv:2311.04400*, 2023.
- [16] Jiayang Tang, Zhaoxi Chen, Xiaokang Chen, Tengfei Wang, Gang Zeng, and Ziwei Liu. Lgm: Large multi-view gaussian model for high-resolution 3d content creation. *arXiv preprint arXiv:2402.05054*, 2024.
- [17] Yinghao Xu, Zifan Shi, Wang Yifan, Hansheng Chen, Ceyuan Yang, Sida Peng, Yujun Shen, and Gordon Wetzstein. Grm: Large gaussian reconstruction model for efficient 3d reconstruction and generation. *arXiv preprint arXiv:2403.14621*, 2024.
- [18] Zhengyi Wang, Yikai Wang, Yifei Chen, Chendong Xiang, Shuo Chen, Dajiang Yu, Chongxuan Li, Hang Su, and Jun Zhu. Crm: Single image to 3d textured mesh with convolutional reconstruction model. *arXiv preprint arXiv:2403.05034*, 2024.
- [19] Jiale Xu, Weihao Cheng, Yiming Gao, Xintao Wang, Shenghua Gao, and Ying Shan. Instantmesh: Efficient 3d mesh generation from a single image with sparse-view large reconstruction models. *arXiv preprint arXiv:2404.07191*, 2024.
- [20] Xianggang Yu, Mutian Xu, Yidan Zhang, Haolin Liu, Chongjie Ye, Yushuang Wu, Zizheng Yan, Chenming Zhu, Zhangyang Xiong, Tianyou Liang, et al. Mvimnet: A large-scale dataset of multi-view images. In *Proceedings of the IEEE/CVF conference on computer vision and pattern recognition*, pages 9150–9161, 2023.
- [21] Jiahao Li, Hao Tan, Kai Zhang, Zexiang Xu, Fujun Luan, Yinghao Xu, Yicong Hong, Kalyan Sunkavalli, Greg Shakhnarovich, and Sai Bi. Instant3d: Fast text-to-3d with sparse-view generation and large reconstruction model. *arXiv preprint arXiv:2311.06214*, 2023.
- [22] Luke Melas-Kyriazi, Iro Laina, Christian Rupprecht, Natalia Neverova, Andrea Vedaldi, Oran Gafni, and Filippos Kokkinos. Im-3d: Iterative multiview diffusion and reconstruction for high-quality 3d generation. *arXiv preprint arXiv:2402.08682*, 2024.
- [23] Qi Zuo, Xiaodong Gu, Lingteng Qiu, Yuan Dong, Zhengyi Zhao, Weihao Yuan, Rui Peng, Siyu Zhu, Zilong Dong, Liefeng Bo, et al. Videomv: Consistent multi-view generation based on large video generative model. *arXiv preprint arXiv:2403.12010*, 2024.
- [24] Weiyu Li, Rui Chen, Xuelin Chen, and Ping Tan. Sweetdreamer: Aligning geometric priors in 2d diffusion for consistent text-to-3d. *arXiv preprint arXiv:2310.02596*, 2023.
- [25] Andreas Blattmann, Tim Dockhorn, Sumith Kulal, Daniel Mendelevitch, Maciej Kilian, Dominik Lorenz, Yam Levi, Zion English, Vikram Voleti, Adam Letts, et al. Stable video diffusion: Scaling latent video diffusion models to large datasets. *arXiv preprint arXiv:2311.15127*, 2023.

- [26] Laura Downs, Anthony Francis, Nate Koenig, Brandon Kinman, Ryan Hickman, Krista Reymann, Thomas B McHugh, and Vincent Vanhoucke. Google scanned objects: A high-quality dataset of 3d scanned household items. In *2022 International Conference on Robotics and Automation (ICRA)*, pages 2553–2560. IEEE, 2022.
- [27] Robin Rombach, Andreas Blattmann, Dominik Lorenz, Patrick Esser, and Björn Ommer. High-resolution image synthesis with latent diffusion models. In *Proceedings of the IEEE/CVF conference on computer vision and pattern recognition*, pages 10684–10695, 2022.
- [28] Chitwan Saharia, William Chan, Saurabh Saxena, Lala Li, Jay Whang, Emily L Denton, Kamyar Ghasemipour, Raphael Gontijo Lopes, Burcu Karagol Ayan, Tim Salimans, et al. Photorealistic text-to-image diffusion models with deep language understanding. *Advances in neural information processing systems*, 35:36479–36494, 2022.
- [29] Dustin Podell, Zion English, Kyle Lacey, Andreas Blattmann, Tim Dockhorn, Jonas Müller, Joe Penna, and Robin Rombach. Sdxl: Improving latent diffusion models for high-resolution image synthesis. *arXiv preprint arXiv:2307.01952*, 2023.
- [30] Axel Sauer, Frederic Boesel, Tim Dockhorn, Andreas Blattmann, Patrick Esser, and Robin Rombach. Fast high-resolution image synthesis with latent adversarial diffusion distillation. *arXiv preprint arXiv:2403.12015*, 2024.
- [31] Jonathan Ho, Tim Salimans, Alexey Gritsenko, William Chan, Mohammad Norouzi, and David J Fleet. Video diffusion models. *Advances in Neural Information Processing Systems*, 35:8633–8646, 2022.
- [32] Jonathan Ho, William Chan, Chitwan Saharia, Jay Whang, Ruiqi Gao, Alexey Gritsenko, Diederik P Kingma, Ben Poole, Mohammad Norouzi, David J Fleet, et al. Imagen video: High definition video generation with diffusion models. *arXiv preprint arXiv:2210.02303*, 2022.
- [33] Uriel Singer, Adam Polyak, Thomas Hayes, Xi Yin, Jie An, Songyang Zhang, Qiyuan Hu, Harry Yang, Oron Ashual, Oran Gafni, et al. Make-a-video: Text-to-video generation without text-video data. *arXiv preprint arXiv:2209.14792*, 2022.
- [34] Xin Ma, Yaohui Wang, Gengyun Jia, Xinyuan Chen, Ziwei Liu, Yuan-Fang Li, Cunjian Chen, and Yu Qiao. Latte: Latent diffusion transformer for video generation. *arXiv preprint arXiv:2401.03048*, 2024.
- [35] Tim Brooks, Bill Peebles, Connor Holmes, Will DePue, Yufei Guo, Li Jing, David Schnurr, Joe Taylor, Troy Luhman, Eric Luhman, Clarence Ng, Ricky Wang, and Aditya Ramesh. Video generation models as world simulators, 2024.
- [36] Chuanxia Zheng and Andrea Vedaldi. Free3d: Consistent novel view synthesis without 3d representation. *arXiv preprint arXiv:2312.04551*, 2023.
- [37] Jiayu Yang, Ziang Cheng, Yunfei Duan, Pan Ji, and Hongdong Li. Consistnet: Enforcing 3d consistency for multi-view images diffusion. *arXiv preprint arXiv:2310.10343*, 2023.
- [38] Ben Mildenhall, Pratul P Srinivasan, Matthew Tancik, Jonathan T Barron, Ravi Ramamoorthi, and Ren Ng. Nerf: Representing scenes as neural radiance fields for view synthesis. *Communications of the ACM*, 65(1):99–106, 2021.
- [39] Jonathan T Barron, Ben Mildenhall, Matthew Tancik, Peter Hedman, Ricardo Martin-Brualla, and Pratul P Srinivasan. Mip-nerf: A multiscale representation for anti-aliasing neural radiance fields. In *Proceedings of the IEEE/CVF International Conference on Computer Vision*, pages 5855–5864, 2021.
- [40] Thomas Müller, Alex Evans, Christoph Schied, and Alexander Keller. Instant neural graphics primitives with a multiresolution hash encoding. *ACM transactions on graphics (TOG)*, 41(4):1–15, 2022.
- [41] Bernhard Kerbl, Georgios Kopanas, Thomas Leimkuehler, and George Drettakis. 3d gaussian splatting for real-time radiance field rendering. *ACM Transactions on Graphics (TOG)*, 42(4):1–14, 2023.
- [42] Hanwen Jiang, Zhenyu Jiang, Yue Zhao, and Qixing Huang. Leap: Liberate sparse-view 3d modeling from camera poses. *arXiv preprint arXiv:2310.01410*, 2023.
- [43] Zi-Xin Zou, Zhipeng Yu, Yuan-Chen Guo, Yangguang Li, Ding Liang, Yan-Pei Cao, and Song-Hai Zhang. Triplane meets gaussian splatting: Fast and generalizable single-view 3d reconstruction with transformers. *arXiv preprint arXiv:2312.09147*, 2023.
- [44] Ben Poole, Ajay Jain, Jonathan T Barron, and Ben Mildenhall. Dreamfusion: Text-to-3d using 2d diffusion. *arXiv preprint arXiv:2209.14988*, 2022.

- [45] Chen-Hsuan Lin, Jun Gao, Luming Tang, Towaki Takikawa, Xiaohui Zeng, Xun Huang, Karsten Kreis, Sanja Fidler, Ming-Yu Liu, and Tsung-Yi Lin. Magic3d: High-resolution text-to-3d content creation. In *Proceedings of the IEEE/CVF Conference on Computer Vision and Pattern Recognition*, pages 300–309, 2023.
- [46] Yuan-Chen Guo, Ying-Tian Liu, Ruizhi Shao, Christian Laforte, Vikram Voleti, Guan Luo, Chia-Hao Chen, Zi-Xin Zou, Chen Wang, Yan-Pei Cao, and Song-Hai Zhang. threestudio: A unified framework for 3d content generation. <https://github.com/threestudio-project/threestudio>, 2023.
- [47] Peng Wang, Lingjie Liu, Yuan Liu, Christian Theobalt, Taku Komura, and Wenping Wang. Neus: Learning neural implicit surfaces by volume rendering for multi-view reconstruction. *arXiv preprint arXiv:2106.10689*, 2021.
- [48] Ruoshi Liu, Rundi Wu, Basile Van Hoorick, Pavel Tokmakov, Sergey Zakharov, and Carl Vondrick. Zero-1-to-3: Zero-shot one image to 3d object. In *Proceedings of the IEEE/CVF International Conference on Computer Vision*, pages 9298–9309, 2023.
- [49] Chong Mou, Xintao Wang, Liangbin Xie, Yanze Wu, Jian Zhang, Zhongang Qi, and Ying Shan. T2i-adapter: Learning adapters to dig out more controllable ability for text-to-image diffusion models. In *Proceedings of the AAAI Conference on Artificial Intelligence*, volume 38, pages 4296–4304, 2024.
- [50] Ting Chen, Ruixiang Zhang, and Geoffrey Hinton. Analog bits: Generating discrete data using diffusion models with self-conditioning. *arXiv preprint arXiv:2208.04202*, 2022.
- [51] Jeff Rasley, Samyam Rajbhandari, Olatunji Ruwase, and Yuxiong He. Deepspeed: System optimizations enable training deep learning models with over 100 billion parameters. In *Proceedings of the 26th ACM SIGKDD International Conference on Knowledge Discovery & Data Mining*, pages 3505–3506, 2020.
- [52] Richard Zhang, Phillip Isola, Alexei A Efros, Eli Shechtman, and Oliver Wang. The unreasonable effectiveness of deep features as a perceptual metric. In *Proceedings of the IEEE conference on computer vision and pattern recognition*, pages 586–595, 2018.
- [53] Dmitry Tochilkin, David Pankratz, Zexiang Liu, Zixuan Huang, Adam Letts, Yangguang Li, Ding Liang, Christian Laforte, Varun Jampani, and Yan-Pei Cao. Tripotr: Fast 3d object reconstruction from a single image. *arXiv preprint arXiv:2403.02151*, 2024.
- [54] Tero Karras, Miika Aittala, Timo Aila, and Samuli Laine. Elucidating the design space of diffusion-based generative models. *Advances in Neural Information Processing Systems*, 35:26565–26577, 2022.
- [55] Lvmin Zhang, Anyi Rao, and Maneesh Agrawala. Adding conditional control to text-to-image diffusion models. In *Proceedings of the IEEE/CVF International Conference on Computer Vision*, pages 3836–3847, 2023.
- [56] Wenzhe Shi, Jose Caballero, Ferenc Huszár, Johannes Totz, Andrew P Aitken, Rob Bishop, Daniel Rueckert, and Zehan Wang. Real-time single image and video super-resolution using an efficient sub-pixel convolutional neural network. In *Proceedings of the IEEE conference on computer vision and pattern recognition*, pages 1874–1883, 2016.
- [57] Kaiming He, Xiangyu Zhang, Shaoqing Ren, and Jian Sun. Deep residual learning for image recognition. In *Proceedings of the IEEE conference on computer vision and pattern recognition*, pages 770–778, 2016.

## A Technical Details

### A.1 Video Model Fine-tuning

Based on the approach outlined in [25], the generation process employs the EDM framework[54]. Let  $p_{\text{data}}(\mathbf{x}_0)$  represent the video data distribution, and  $p(\mathbf{x}; \sigma)$  be the distribution obtained by adding Gaussian noise with variance  $\sigma^2$  to the data. For sufficiently large  $\sigma_{\text{max}}$ ,  $p(x; \sigma_{\text{max}}^2)$  approximates a normal distribution  $\mathcal{N}(0, \sigma_{\text{max}}^2)$ . Diffusion models (DMs) leverage this property and begin with high variance Gaussian noise,  $x_M \sim \mathcal{N}(0, \sigma_{\text{max}}^2)$ , and then iteratively denoise the data until reaching  $\sigma_0 = 0$ .

In practice, this iterative refinement process can be implemented through the numerical simulation of the Probability Flow ordinary differential equation (ODE):

$$d\mathbf{x} = -\dot{\sigma}(t)\sigma(t)\nabla_{\mathbf{x}} \log p(\mathbf{x}; \sigma(t)) dt \quad (3)$$

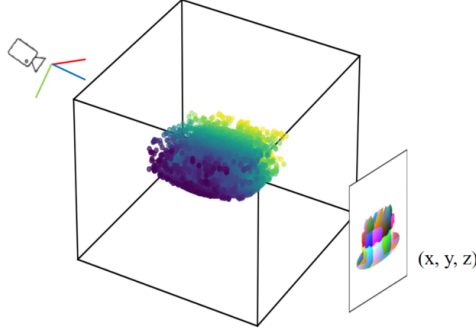


Figure 9: The projection process of coordinates map.

where  $\nabla_{\mathbf{x}} \log p(\mathbf{x}; \sigma)$  is called as score function.

DM training is to learn a model  $s_{\theta}(\mathbf{x}; \sigma)$  to approximate the score function  $\nabla_{\mathbf{x}} \log p(\mathbf{x}; \sigma)$ . The model can be parameterized as:

$$\nabla_{\mathbf{x}} \log p(\mathbf{x}; \sigma) \approx s_{\theta}(\mathbf{x}; \sigma) = \frac{D_{\theta}(\mathbf{x}; \sigma) - \mathbf{x}}{\sigma^2}, \quad (4)$$

where  $D_{\theta}$  is a learnable denoiser that aims to predict ground truth  $\mathbf{x}_0$ .

The denoiser  $D_{\theta}$  is trained via denoising score matching (DSM):

$$\mathbb{E}_{\mathbf{x}_0 \sim p_{\text{data}}(\mathbf{x}_0), (\sigma, n) \sim p(\sigma, n)} [\lambda_{\sigma} \|D_{\theta}(\mathbf{x}_0 + n; \sigma) - \mathbf{x}_0\|_2^2], \quad (5)$$

where  $p(\sigma, n) = p(\sigma)\mathcal{N}(n; 0, \sigma^2)$ ,  $p(\sigma)$  is a distribution over noise levels  $\sigma$ ,  $\lambda_{\sigma}$  is a weighting function. The learnable denoiser  $D_{\theta}$  is parameterized as:

$$D_{\theta}(\mathbf{x}; \sigma) = c_{\text{skip}}(\sigma)\mathbf{x} + c_{\text{out}}(\sigma)F_{\theta}(c_{\text{in}}(\sigma)\mathbf{x}; c_{\text{noise}}(\sigma)), \quad (6)$$

where  $F_{\theta}$  is the network to be trained.

We sample  $\log \sigma \sim \mathcal{N}(P_{\text{mean}}, P_{\text{std}}^2)$ , with  $P_{\text{mean}} = 1.0$  and  $P_{\text{std}} = 1.6$ . Then we obtain all the parameters as follows:

$$c_{\text{in}} = \frac{1}{\sqrt{\sigma^2 + 1}} \quad (7)$$

$$c_{\text{out}} = \frac{-\sigma}{\sqrt{\sigma^2 + 1}} \quad (8)$$

$$c_{\text{skip}}(\sigma) = \frac{1}{\sigma^2 + 1} \quad (9)$$

$$c_{\text{noise}}(\sigma) = 0.25 \log \sigma \quad (10)$$

$$\lambda(\sigma) = \frac{1 + \sigma^2}{\sigma^2} \quad (11)$$

We fine-tune the network backbone  $F_{\theta}$  on multi-view images of size  $512 \times 512$ . During training, for each instance in the dataset, we uniformly sample 8 views and choose the first view as the input view. view images of size  $512 \times 512$ .

## A.2 Canonical Coordinates Map

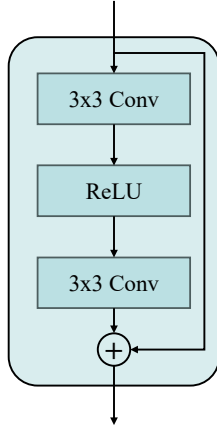
For control networks [55, 49] of image diffusion models, the conditional maps like depth maps need to be normalized to  $[0, 1]$ , typically using the formula:  $(p - p_{\text{mean}})/(p_{\text{max}} - p_{\text{min}})$ . For multi-view generation, each view performs a normalize operation on itself, which results in a scale ambiguity. At the same time, the depth map is relative to a certain view, and the correlation between the depth values is not significant across views.

To avoid the above issues caused by self-normalization, we use canonical coordinate maps (CCM). Coordinate maps transform the depth value  $d$  to a common world coordinate system using the camera’s intrinsic and extrinsic parameters, represented as  $(X, Y, Z)$ . The transformation formula is:

$$\begin{pmatrix} X \\ Y \\ Z \end{pmatrix} = K^{-1} \cdot \begin{pmatrix} u \\ v \\ 1 \end{pmatrix} \cdot d$$

where  $(u, v)$  are the pixel coordinates,  $d$  is the corresponding depth value, and  $K$  is the camera intrinsic matrix. Then the coordinate values of all views will be multiplied by a **global** scale and added an offset value to convert to the range of 0 to 1. This representation makes the correlation between different views more significant and is helpful for multi-view generation.

### A.3 3D-aware Feedback



| Input               | inp $\in \mathbb{R}^{3 \times 512 \times 512}$ |
|---------------------|--|
| PixelUnshuffle [56] | $192 \times 64 \times 64$                      |
| ResBlock $\times 3$ | $320 \times 64 \times 64$                      |
| ResBlock $\times 3$ | $640 \times 32 \times 32$                      |
| ResBlock $\times 3$ | $1280 \times 16 \times 16$                     |
| ResBlock $\times 3$ | $1280 \times 8 \times 8$                       |

Table 3: The detailed structure of all layers in the feedback injection network.

Figure 10: Architecture of the residual block used in the feedback stage.

With reference to Section 3.3 in the main paper, Fig. 10 and Table 3 provide a detailed illustration of the feedback injection network. We use two networks to inject the coordinates map and RGB texture map feedback into the score function. Each network consists of four feature extraction blocks and three downsample blocks to adjust the feature resolution. The reconstruction coordinates map and RGB texture map initially have a resolution of  $512 \times 512$ . We employ the pixel unshuffle operation to downsample these maps to  $64 \times 64$ .

At each scale, three residual blocks[57] are used to extract the multi-scale feedback features, denoted as  $F_P = \{F_p^1, F_p^2, F_p^3, F_p^4\}$  and  $F_T = \{F_t^1, F_t^2, F_t^3, F_t^4\}$  for the coordinates map and RGB texture map, respectively. These feedback features match the intermediate features  $F_{enc} = \{F_{enc}^1, F_{enc}^2, F_{enc}^3, F_{enc}^4\}$  in the encoder of the UNet denoiser. The feedback features  $F_P$  and  $F_T$  are added to the intermediate features  $F_{enc}$  at each scale as described by the following equations:

$$\mathbf{F}_p = \mathcal{F}^0(P) \tag{12}$$

$$\mathbf{F}_t = \mathcal{F}^1(T) \tag{13}$$

$$\mathbf{F}_{enc}^i = \mathbf{F}_{enc}^i + \mathbf{F}_p^i + \mathbf{F}_t^i, \quad i \in \{1, 2, 3, 4\} \tag{14}$$

where  $P$  represents the coordinates map feedback input, and  $T$  represents the RGB texture feedback input.  $\mathcal{F}^0$  and  $\mathcal{F}^1$  denote the functions of the feedback inject network applied to the coordinates map and RGB texture map, respectively.